Oxid Met (2011) 76:93–109
DOI 10.1007/s11085-011-9240-z

ORIGINAL PAPER

The Effects of KCl, K_2SO_4 and K_2CO_3 on the High Temperature Corrosion of a 304-Type Austenitic Stainless Steel

Jesper Pettersson · Nicklas Folkeson · Lars-Gunnar Johansson · Jan-Erik Svensson

Received: 20 June 2010 / Revised: 2 December 2010 / Published online: 11 March 2011

Abstract The oxidation of 304-type (Fe18Cr10Ni) austenitic stainless steel was investigated at 500 and 600 °C in 5% O_2 + 40% H_2O. Prior to exposure the samples were sprayed with KCl, K_2CO_3 or K_2SO_4, the amount of salt corresponding to 1.35 μmol K^+/cm^2. For reference, salt-free samples were exposed in 5% O_2 + 40% H_2O and in 5% O_2 (N_2 was used as carrier gas). The oxidized samples were analyzed with SEM/EDX, XRD, IC and FIB. KCl and K_2CO_3 strongly accelerate the corrosion of 304L while K_2SO_4 has little influence on the corrosion rate and on the morphology of the corroded surface. KCl and K_2CO_3 react with the chromium-rich oxide on the sample surface, forming K_2CrO_4. The resulting chromium depletion of the protective oxide causes rapid oxidation and the formation of a thick duplex scale consisting of an outer hematite layer and a inner layer made up of FeCrNi spinel-type oxide. The differences in the corrosivity of the three salts are directly connected to their ability to form chromate on the surface and, hence, to the relative stability of the corresponding leaving groups (HCl, CO_2 and SO_3).

Keywords KCl induced corrosion · K_2SO_4 · Deposit · Waste · Biomass · 304L

J. Pettersson (✉) · N. Folkeson · L.-G. Johansson · J.-E. Svensson
Department of Chemical and Biological Engineering, Energy and Materials, Chalmers University of Technology, 412 96, Göteborg, Sweden
e-mail: jpetter@chalmers.se

N. Folkeson
e-mail: nicklas.folkeson@chalmers.se

L.-G. Johansson
e-mail: lg@chalmers.se

J.-E. Svensson
e-mail: jes@chalmers.se

Introduction

The production of electricity from biomass and waste fired power plants is an attractive alternative to using fossil fuels because the burning of biomass makes no net contribution of CO_2 to the atmosphere. However, the tendency of these fuels to cause fireside corrosion on the steam superheaters is a major problem, especially in waste-fired plants. In order to limit the degradation of the superheaters, biomass and waste-fired plants are operated at a considerably lower maximum steam temperature than fossil-fuelled power plants. As a result, the electricity generating efficiency is greatly diminished. To increase the maximum steam temperature in biomass and waste-fired plants it is necessary to improve the corrosion resistance of the alloys or to mitigate the corrosive fireside environment.

In many cases, the superheaters are made from FeCr and FeCrNi alloys that rely on the formation of a chromium-rich oxide of corundum type, Me_2O_3, for corrosion protection. The protective oxide is usually a solid solution of iron and chromium oxide (i.e. $Fe_{2-x}Cr_xO_3$) and the properties of this oxide depend on the chromia content, where oxides with a high Cr/Fe ratio are more protective. Hence, processes that deplete the oxide in chromium tend to be harmful, leading to an iron rich oxide with poor protective properties. It has been shown previously, that the reaction of $O_2 + H_2O$ mixtures with the protective oxide to form gaseous chromic acid (H_2CrO_4) is such a process [1–3]. Thus, in the case of alloy 304L exposed in $O_2 + H_2O$, the result is local breakaway corrosion with a duplex oxide consisting of an outward growing hematite layer and inward growing spinel oxide [4].

The combustion of biomass and waste generates a fireside environment which is rich in alkali, chlorine and calcium whereas the SO_2 content is low [5–8]. Hence, the deposits formed on the superheater tubes are often rich in alkali chlorides. The corrosivity of alkali chlorides towards stainless steels at high temperature is well documented [9–16]. Hence, several attempts have been made to mitigate corrosion in the boilers by changing the chemistry of the fireside environment so as to suppress the formation of alkali chloride deposits [5, 6, 17–19]. These attempts have had some success. Thus, it has been reported that the addition of sulphur or sulphur-containing compounds to the fuel resulted in 50–70% decrease in corrosion rate of probe exposed samples. The mitigation of corrosion was attributed to the partial replacement of alkali chlorides by alkali sulphates in the deposit.

It may be noted that the corrosivity of alkali chlorides is usually attributed to the chloride ion [9–13]. Thus, most workers invoke the so-called "active oxidation" mechanism to explain the corrosivity of these salts. In this scenario, Cl_2 plays a crucial catalytic role in the corrosion process by generating volatile metal chlorides. However, recent work on the KCl-induced high temperature corrosion of stainless steel at this laboratory indicates that the potassium ion plays the most important part in the initial stages of corrosion [20–23].

The present study is intended to elucidate the role of the alkali ion (i.e. potassium) in the high temperature corrosion of stainless steels. Hence, we have performed a comparative study of the high temperature corrosion effects of KCl, K_2CO_3 and K_2SO_4 on 304L type steel. The idea is to show whether the chloride ion

is really essential for corrosion to occur and to investigate the corrosion effects of potassium carbonate and potassium sulphate.

Experimental Procedures

The material used in the study was the austenitic stainless steel, 304L (Table 1). The geometrical area of the samples was 15 × 15 × 2 mm^3. A hole ($\phi = 1.5$ mm) was drilled for easy handling. Before exposure the samples were grinded to 1000 grit SiC and polished with 1 μm diamond spray until a mirror-like surface appeared. The polished samples were degreased and cleaned in acetone and ethanol using an ultrasonic bath. Salt was applied by spraying the samples with a saturated solution of the desired salt in water, water/ethanol or acetone. The amount of salt corresponded to a potassium content of 1.35 μmol K^+/cm^2 (0.10 mg/cm^2 in the case of KCl). The samples were dried with cool air and subsequently exposed in the thermobalance. The temperature was kept at 500 and 600 °C (±1 °C). The experiments were carried out in 5% O_2 + 40% H_2O (or 5% O_2 in the reference run) and the flow rate was set to 2.5 cm/s. Nitrogen was used as carrier gas. To obtain 40% water vapour concentration the mixed gas was led through a humidifier and a temperature controlled condenser (Fig. 1).

Corrosion Product Characterization

Scanning Electron Microscopy (SEM)

The oxide scales were examined with a Leo Ultra 55 SEM and an FEI Quanta 200 FEG ESEM. The SEMs have field emission electron guns (FEG) and are equipped with Oxford Inca energy dispersive X-ray (EDX) systems. SEM/EDX was used for elemental mapping and quantification. For imaging and EDX analysis an accelerating voltage of 20 kV was used.

Focused Ion Beam (FIB) Microscopy

In order to create cross-sections of the oxide scale and the subjacent metal an FEI FIB 200 THP focused ion beam (FIB) workstation and an FEI Strata DB 235 M combined FIB/SEM system were used. The FIB/SEM is a dual beam system, i.e. it has both an electron column and an ion column. The electron column is equipped with a FEG and the ion column has a liquid gallium source. The FEI FIB 200 THP workstation is also equipped with a liquid gallium source.

Table 1 Chemical composition of alloy 304L in weight %

	Fe	Cr	Ni	Mn	Si	Mo	N	C
304L	Balance	18.5	10.2	1.41	0.55	0.49	0.075	0.027

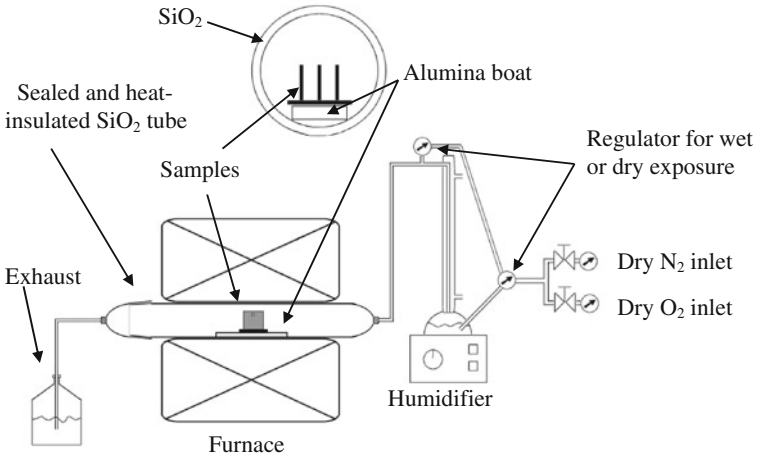

Fig. 1 Experimental setup for exposures in a horizontal silica furnace

X-Ray Diffraction (XRD)

To analyze any crystalline corrosion products formed the Grazing-Incidence X-ray diffraction (GI-XRD) technique was used. The diffractometer was a Siemens D5000 powder diffractometer, equipped with grazing incidence beam attachment and a Göbel mirror. Cu K_α radiation was used and the angle of incidence was 2°. The measuring range of the detector was $10° < 2\theta < 65°$.

Ion Chromatography (IC)

To determine the amount of water-soluble cations (K^+) and anions (Cl^-, SO_4^{2-} and CrO_4^{2-}), two Dionex 100 systems were used. The cations were analysed with an IonPac CS12A analytic column and 20 mM sulfonic acid was used as eluent. The anions were analysed with an IonPac AS4A-SC analytic column and 1.8 mM Na_2CO_3/1.7 mM $NaHCO_3$ was used as eluent. The flow rate was 2 ml/min for both cations and anions. In the anion analysis, a Dionex OnGuard IIH was used to separate alkali metal ions and transition metals before introducing the sample to the column. The samples were leached in 2 × 10 ml MilliQ water using ultrasonic agitation for 1 + 10 min.

Results

Gravimetry

Figures 2 and 3 show mass gain as a function of exposure time for 304L exposed in O_2 + 40% H_2O at 500 and 600 °C in the presence of KCl, K_2CO_3 and K_2SO_4. Reference exposures were carried out in the absence of salt (dry O_2 and O_2 + 40%

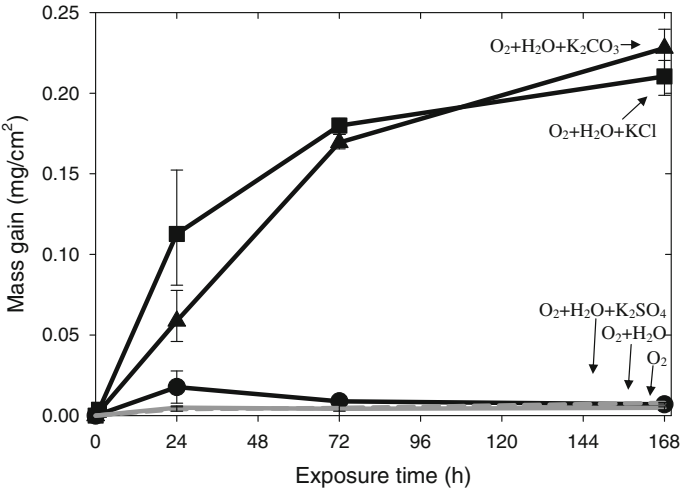

Fig. 2 Mass gain versus exposure time for samples exposed at 500 °C in O_2, $O_2 + H_2O$, $O_2 + H_2O + KCl$, $O_2 + H_2O + K_2CO_3$ and $O_2 + H_2O + K_2SO_4$. The amount of applied salt corresponded to 1.35 μmol K^+/cm^2

H_2O) and are also shown. Firstly, it may be noted that mass gain at 600 °C is greatly increased by water vapour in the absence of salt, see Fig. 3. Thus, after 168 h at 600 °C in the absence of salt, mass gain is 25 times higher in $O_2 + H_2O$ environment compared to dry O_2. In contrast, water vapour has no effect on mass gain at 500 °C, see Fig. 2. Considering their effect on mass gain, the salts investigated fall in two categories. Thus, at 500 and 600 °C the presence of KCl and K_2CO_3 resulted in much greater mass gains while the presence of K_2SO_4 did not increase mass gain. At 500 °C, the effect of KCl on mass gain is initially somewhat greater than for K_2CO_3, see Fig. 2. This difference has disappeared after 168 h, the mass gains recorded being similar for the samples exposed in the presence of KCl and K_2CO_3, respectively. At 600 °C, KCl and K_2CO_3 initially accelerates mass gain equally much, see Fig. 3. However, after 168 h exposure in the presence of K_2CO_3 mass gain was almost 50% higher than in the corresponding KCl exposure. It may be noted that K_2SO_4 had negligible effect on mass gain at 500 °C. At 600 °C, the mass gain of the sample exposed in the presence of K_2SO_4 is similar to the mass gain of the corresponding sample exposed in the ($O_2 + H_2O$), during the first 72 h. However, between 72 and 168 h the mass gain of the sample exposed in the presence of K_2SO_4 is less than in the reference case. After 168 h exposure the mass gain of the K_2SO_4 exposed sample is almost 3 times lower compared to the reference exposed sample.

Regardless of exposure, the highest mass gain was always detected for the samples exposed at 600 °C. The effect of temperature is most pronounced in the reference run in $O_2 + H_2O$ environment where mass gain was more than 100 times greater at 600 °C than at 500 °C.

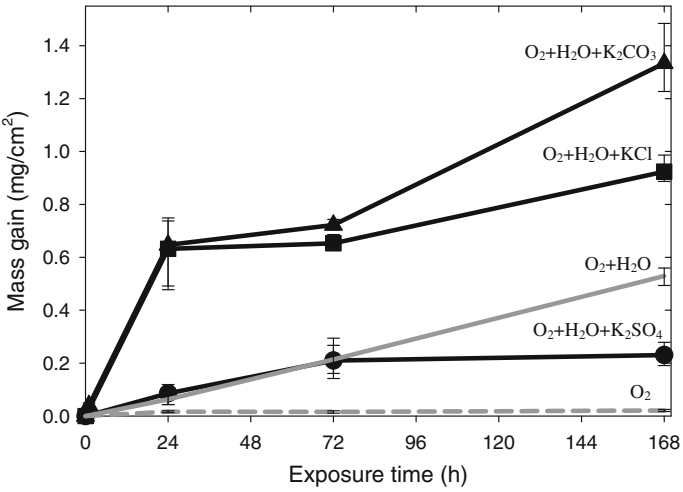

Fig. 3 Mass gain versus exposure time for samples exposed at 600 °C in O_2, $O_2 + H_2O$, $O_2 + H_2O + KCl$, $O_2 + H_2O + K_2CO_3$ and $O_2 + H_2O + K_2SO_4$. The amount of applied salt corresponded to 1.35 μmol K^+/cm^2

Scale Morphology by SEM

Oxidation in dry O_2 at 500 and 600 °C in the absence of salt resulted in the formation of a smooth and protective oxide, see Fig. 4a, b. This is also the case in $O_2 + H_2O$ environment at 500 °C, see Fig. 4c. The contrast in the images is due to small lateral variations in the thickness and morphology of the oxide, mirroring the grain structure of the steel. The protective behaviour is in accordance with the very small mass gains recorded (see Figs. 2, 3). In contrast, oxidation in $O_2 + H_2O$ at 600 °C in the absence of salt resulted in the formation of oxide islands on the surface, see Fig. 4d. The oxide islands form on the middle of some of the steel grains, other grains and the area close to steel grain boundaries remaining smooth.

Samples exposed for 24 h in $O_2 + H_2O + KCl$ environment are shown in Fig. 4e (500 °C) and Fig. 4f (600 °C). After 24 h at 500 °C, the corroded surface can be described in terms of two characteristic morphologies. Most of the surface is covered by a relatively thick scale covering containing numerous dark grey spots. In addition, more or less reacted KCl crystallites are conspicuous on the surface. Thus, Fig. 4e shows an almost unreacted KCl in the left part of the image while partly reacted KCl crystallites, covered by irregular oxide, can be seen in the bottom right part of the image. Exposure for 24 h at 600 °C resulted in a scale morphology which is similar to that described for 500 °C. Thus, there is a rather thick scale with scattered oxide agglomerates corresponding to the KCl crystallites deposited before exposure. At this stage, KCl is absent (see XRD analysis below), all KCl crystallites having reacted or evaporated. The oxide agglomerates tend to be hollow (see below) and have approximately the same size and shape as the former KCl crystals. Exposure in $O_2 + H_2O + K_2CO_3$ environment resulted in surface morphologies similar to those formed in the presence of KCl, see Fig. 4g (500 °C) and 4 h

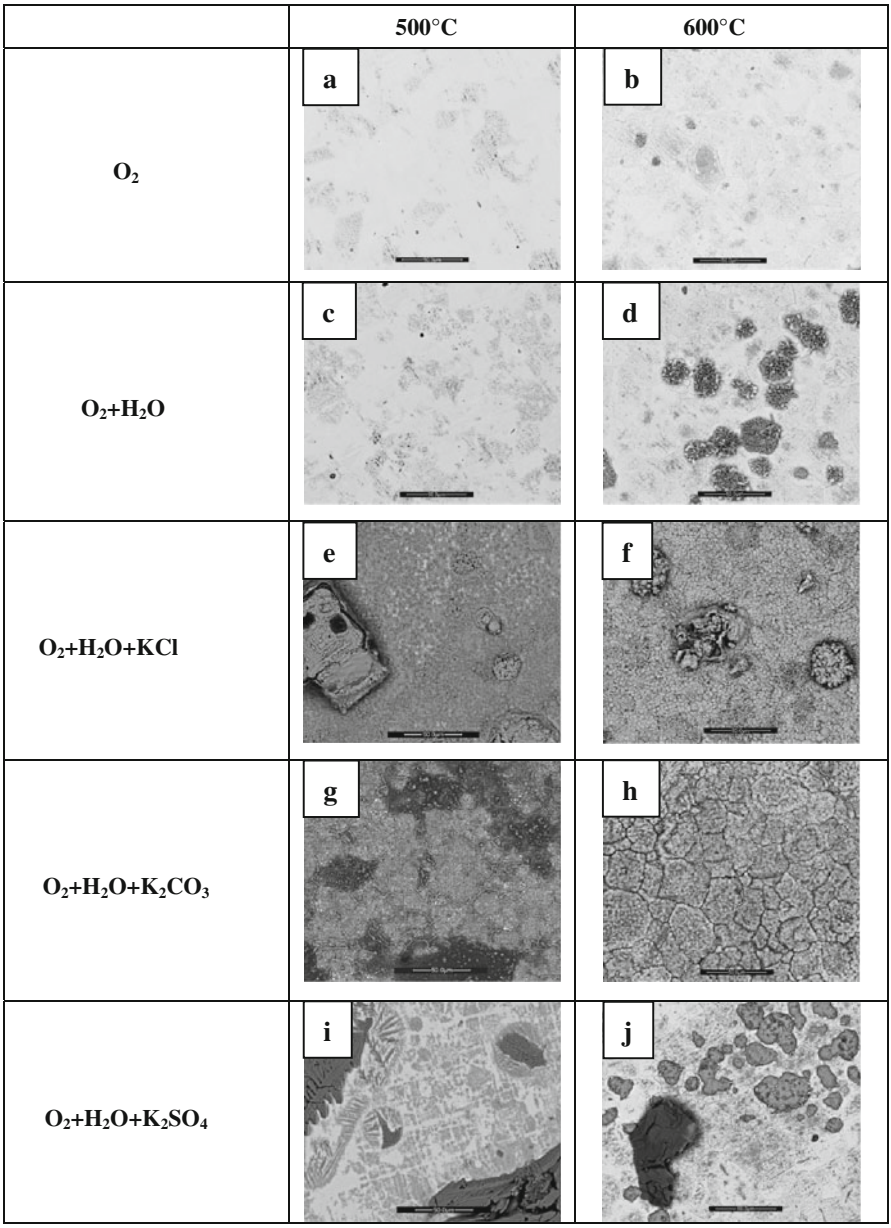

Fig. 4 SEM images with a scale bar corresponding to 50 μm. The samples are oxidized for 24 h at 500 and 600 °C in (**a** and **b**) O_2 (**c** and **d**) $O_2 + H_2O$ (**e** and **f**) $O_2 + H_2O + KCl$ (**g** and **h**) $O_2 + H_2O + K_2CO_3$ (**i** and **j**) $O_2 + H_2O + K_2SO_4$

(600 °C). At 500 °C, a relatively thick continuous scale has formed with agglomerations of partly reacted K_2CO_3 on top. At 600 °C a thick undulating scale has formed and there is little evidence for unreacted salt after exposure.

In contrast to the corresponding KCl exposures, there is no evidence for corrosion product agglomerates forming at the position of the original K_2CO_3 crystallites. In contrast to KCl and K_2CO_3, the presence of K_2SO_4 has little influence on the morphology of the oxidized surface; see Fig. 4i (500 °C) and Fig. 4j (600 °C). Thus, unreacted K_2SO_4 particles are present on the surface after exposure at both temperatures and the morphology of the surface between the K_2SO_4 crystallites is essentially the same as in the absence of salt (compare Fig. 4c, d with Fig. 4i, j).

Phase Composition by XRD

Tables 2 and 3 shows the crystalline phases detected on the samples after 24 h exposure at 500 and 600 °C, respectively. In the environments where mass gains were very small (500 °C dry O_2, $O_2 + H_2O$ and $O_2 + H_2O + K_2SO_4$, 600 °C dry O_2), the only crystalline product detected was the corundum-type solid solution $(Cr,Fe)_2O_3$. The low intensity of the oxide peaks and the strong signal from the underlying steel is in accordance with the evidence from gravimetry and microscopy, showing the presence of a very thin oxide. It may be noted that all three salts added before exposure are still detected after 24 h at 500 °C. In contrast, the only salt remaining after exposure at 600 °C was K_2SO_4. Thus, at 600 °C, KCl and K_2CO_3 have both reacted/evaporated from the surface. In the exposures resulting in relatively rapid corrosion/mass gain, the corrosion products identified always included hematite (Fe_2O_3) and spinel type oxide (Me_3O_4). In addition, exposure in the presence of KCl and K_2CO_3 always resulted in the formation of potassium chromate, K_2CrO_4. The samples exposed at 600 °C in the presence of KCl and K_2CO_3 did not give any diffraction from the substrate, indicating the presence of a thick scale.

Analysis of Water Soluble Compounds by Ion Chromatography (IC)

Tables 4 and 5 show the amount of water-soluble anions (Cl^-, SO_4^{2-} and CrO_4^{2-}) and potassium ions detected by Ion Chromatography (IC) analysis after 24 h exposure at 500 and 600 °C. The analysis by IC is in agreement with the XRD results. Thus, in the cases where K_2CrO_4 was detected by XRD, significant amounts of soluble chromate were found by IC. This was the case for the samples exposed in

Table 2 XRD of samples exposed in the presence of KCl, K_2CO_3 or K_2SO_4 at 500 °C for 24 h

	KCl	K_2SO_4	K_2CO_3	K_2CrO_4	Me_3O_4	$(Cr,Fe)_2O_3$	Fe_2O_3	Steel
O_2						W		S
$O_2 + H_2O$						W		S
$O_2 + H_2O + KCl$	S			S	W		M	M
$O_2 + H_2O + K_2CO_3$			W	S	W		M	S
$O_2 + H_2O + K_2SO_4$		S				W		S

The salt treated samples were exposed in 5% O_2 + 40% H_2O. *W* weak, *M* medium, *S* strong intensity peak

Table 3 XRD of samples exposed in the presence of KCl, K_2CO_3 or K_2SO_4 at 600 °C for 24 h

	KCl	K_2SO_4	K_2CO_3	K_2CrO_4	Me_3O_4	$(Cr,Fe)_2O_3$	Fe_2O_3	Steel
O_2						W		S
$O_2 + H_2O$					M		M	S
$O_2 + H_2O + KCl$				W	W		S	
$O_2 + H_2O + K_2CO_3$				W	W		S	
$O_2 + H_2O + K_2SO_4$		M			W		M	S

The salt treated samples were exposed in 5% O_2 + 40% H_2O. *W* weak, *M* medium, *S* strong intensity peak

Table 4 Water soluble ions after exposure for samples exposed in the presence of KCl, K_2CO_3 or K_2SO_4 at 500 °C for 24 h

	$O_2 + H_2O + KCl$	$O_2 + H_2O + K_2CO_3$	$O_2 + H_2O + K_2SO_4$
Amount of anions remaining (percent of added)	32% Cl^-	N/a	86% SO_4^{2-}
Amount of cations remaining (percent of added)	58% K^+	55% K^+	83% K^+
Chromate (CrO_4^{2-}) formation (percent of theoretical yield)	30% CrO_4^{2-}	33% CrO_4^{2-}	0% CrO_4^{2-}
Amount of salt not accounted for because of, e.g. evaporation 100% (%K^+)	42%	45%[b]	17%
Proposed mass balance	28% KCl(s)	22% K_2CO_3(s)	85% K_2SO_4(s)
	42% KCl(g)[a]	45% K_2CO_3(g)[b]	15% spalled K_2SO_4
	30% K_2CrO_4(s)	33% K_2CrO_4(s)	
	4% $MeCl_x$(s)		

The salt treated samples were exposed in 5% O_2 + 40% H_2O

[a] KCl may also evaporate as KOH(g) + HCl(g)

[b] Probably evaporated as KOH(g) + CO_2(g)

the presence of KCl and K_2CO_3 at both 500 and 600 °C. In comparison to the maximum amount of chromate that may be formed (considering that all K^+ added is converted to K_2CrO_4) the yield is in the range 20–30%. In contrast, K_2CrO_4 was not detected on the samples exposed in the presence of K_2SO_4. As a consequence, most (75–85%) of the K_2SO_4 added remained unreacted on the surface during the exposure. The K_2SO_4 not accounted for is considered to have been lost during exposure and handling because of its powdery nature and poor adherence to the sample surface. The difference between the analysis for potassium and sulphate reflects the accuracy of the analysis.

As the chromate detected only corresponds to part of the KCl and K_2CO_3 added before exposure, we also have to account for the remaining fraction of the salts. Let us first consider the exposure with KCl at 600 °C (Table 5). In this case, the relative amounts of K^+ and chromate detected are in accordance with the presence of K_2CrO_4. Lacking any supporting evidence from XRD and SEM/EDX, the small

Table 5 Water soluble ions after exposure for samples exposed in the presence of KCl, K_2CO_3 or K_2SO_4 at 600 °C for 24 h

	$O_2 + H_2O + KCl$	$O_2 + H_2O + K_2CO_3$	$O_2 + H_2O + K_2SO_4$
Amount of anions remaining (percent of added)	1% Cl^-	N/a	73% SO_4^{2-}
Amount of cations remaining (percent of added)	28% K^+	44% K^+	76% K^+
Chromate (CrO_4^{2-}) formation (percent of theoretical yield)	33% CrO_4^{2-}	20% CrO_4^{2-}	0% CrO_4^{2-}
Amount of salt not accounted for because of, e.g. evaporation 100% (%K^+)	72%	56%[b]	24%
Proposed mass balance	0% KCl(s) 72% KCl(g)[a] 33% K_2CrO_4(s) 1% $MeCl_x$(s)	24% K_2CO_3(s) 56% K_2CO_3(g)[b] 20% K_2CrO_4(s)	75% K_2SO_4(s) 25% spalled K_2SO_4

The salt treated samples were exposed in 5% O_2 + 40% H_2O

[a] KCl may also evaporate as KOH(g) + HCl(g)

[b] Probably evaporated as KOH(g) + CO_2(g)

amount of chloride remaining on the surface can be attributed either to KCl or to transition metal chlorides (e.g. $FeCl_2$). This implies that a large fraction of KCl (about 70%) has left the surface. Considering the relatively high vapour pressure of KCl at 600 °C (3.3×10^{-6} bar), it is suggested that most of this has been vaporized. Accordingly, the relatively large fraction of chloride remaining after the corresponding exposure at 500 °C is attributed to the lower vapour pressure of KCl ($pKCl_{eq} = 7.4 \times 10^{-8}$ bar). In the case of potassium carbonate, a relatively large fraction of the potassium added was detected after exposure. Considering the amount of chromate detected, it can be concluded that relatively large fractions of unreacted potassium carbonate remain on the surface after exposure. The greater tendency of potassium carbonate to remain on the surface compared to KCl at 600 °C is explained by its smaller vapour pressure.

SEM/EDX on FIB Cross Sections

After exposure for 24 h in $O_2 + H_2O + KCl$, $O_2 + H_2O + K_2CO_3$ and $O_2 + H_2O + K_2SO_4$ environments at 600 °C the microstructure of the corroded surface was investigated by means of FIB cross sections and SEM/EDX, see Figs. 5, 6 and 7. The top image in Fig. 5 shows the corroded surface after the $O_2 + H_2O + KCl$ exposure and the location of the FIB cross section. The scale surface is rather uneven and oxide whiskers/blades have formed. The cross section was covered by platinum in order to protect the scale surface during FIB milling (the white area on top of the scale in the BSE image in Fig. 5). The EDX maps in Fig. 5 show that a 5–8 μm thick duplex scale has formed. The outer part of the scale consists of relatively pure iron oxide (35% Fe, 1% Cr and 64% O according to the EDX quantification) while the inner layer is rich in chromium and iron and contains

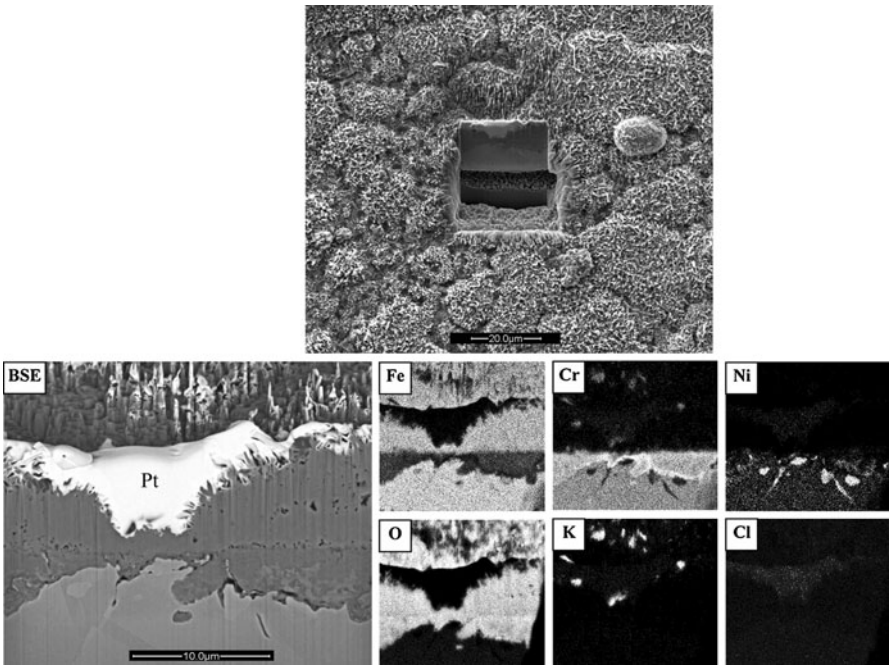

Fig. 5 52° Tilted FIB cross section of a sample exposed at 600 °C in $O_2 + H_2O + KCl$ for 24 h. *Top*: Overview SE image. Micron bar corresponds to 20 µm. *Bottom*: SEM/EDX maps of the cross section. Micron bar corresponds to 10 µm

some nickel (16% Fe, 16% Cr, 7% Ni and 60% O). This is in agreement with the XRD analysis which detected hematite, Fe_2O_3 and spinel type oxide (see Table 3). On top of the scale, areas rich in potassium and chromium were detected, corresponding to the K_2CrO_4 detected by XRD (see Table 3). Below the scale/metal interface there are areas where chromium is depleted and nickel is enriched. These areas are discontinuous and they are partly associated with steel grain boundaries.

Figure 6 shows a FIB cross section of a sample exposed in $O_2 + H_2O + K_2CO_3$ at 600 °C for 24 h. The overview image reveals an undulating scale surface containing dark spots. The EDX mapping shows that the spots consist of potassium, chromium, carbon and oxygen. The identification of K_2CrO_4 by XRD allows us to conclude that these spots contain potassium chromate. In accordance with the IC analysis (see above), the carbon found by EDX is attributed to unreacted potassium carbonate. The scale is similar to that described for the sample exposed in the presence of KCl, the scale being duplex with an outer iron rich part (almost pure Fe_2O_3) and an inner part consisting of iron, chromium and nickel corresponding to the spinel type oxide identified by XRD. Scale thickness is between 6 and 9 µm. A metallic inclusion can be seen in the bottom part of the scale. There are large voids in the middle of the duplex scale, i.e., at the interface between the bottom and top oxide layers. The voids often contain relatively large facetted crystallites with octahedral habitus, presumably consisting of Fe_3O_4. The presence of these crystals within the oxide layers indicates high diffusivity of ions.

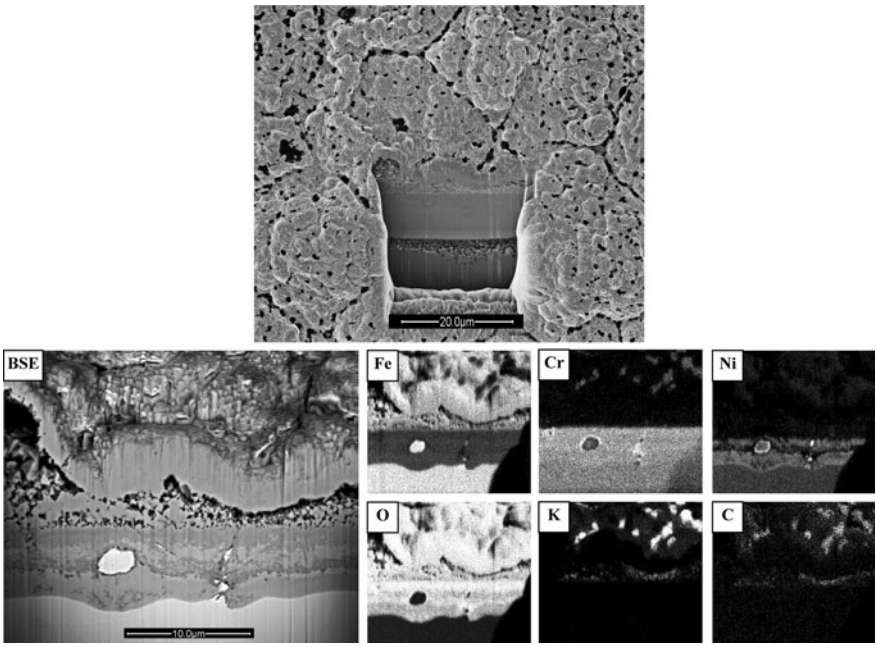

Fig. 6 52° Tilted FIB cross section of a sample exposed at 600 °C in $O_2 + H_2O + K_2CO_3$ for 24 h. *Top*: Overview FIB image. Micron bar corresponds to 20 µm. *Bottom*: SEM/EDX maps of the cross section. Micron bar corresponds to 10 µm

Figure 7 shows a FIB cross section of a corroded sample after 24 h exposure to $O_2 + H_2O + K_2SO_4$ at 600 °C. In contrast to the samples exposed in the presence of KCl and K_2CO_3, there is no thick continuous scale covering the surface. Instead, most of the surface is still covered by a smooth and protective oxide. However, as in the corresponding exposure in the absence of salt, oxide islands have formed on some steel grains. As indicated in the overview image, the FIB cross section was prepared through a part of the surface that included the thin protective oxide and an oxide island with a salt particle on top. EDX analysis showed that the salt particle consisted of unreacted K_2SO_4. The oxide island consists of almost pure iron oxide according to EDX. Beneath the oxide island, an oxide crater containing Cr, Fe and Ni is present. The aggregated thickness of island oxide and crater oxide is 3–4 µm. The island/crater scale morphology is essentially the same as that formed in $O_2 + H_2O$ environment in the absence of salt and corresponds to the duplex hematite/spinel scale formed in the presence of KCl and K_2CO_3 (see above).

Discussion

The present study shows that K_2CO_3 is equally corrosive as KCl towards 304L stainless steel at 500 and 600 °C. This proves that the crucial role in accelerating

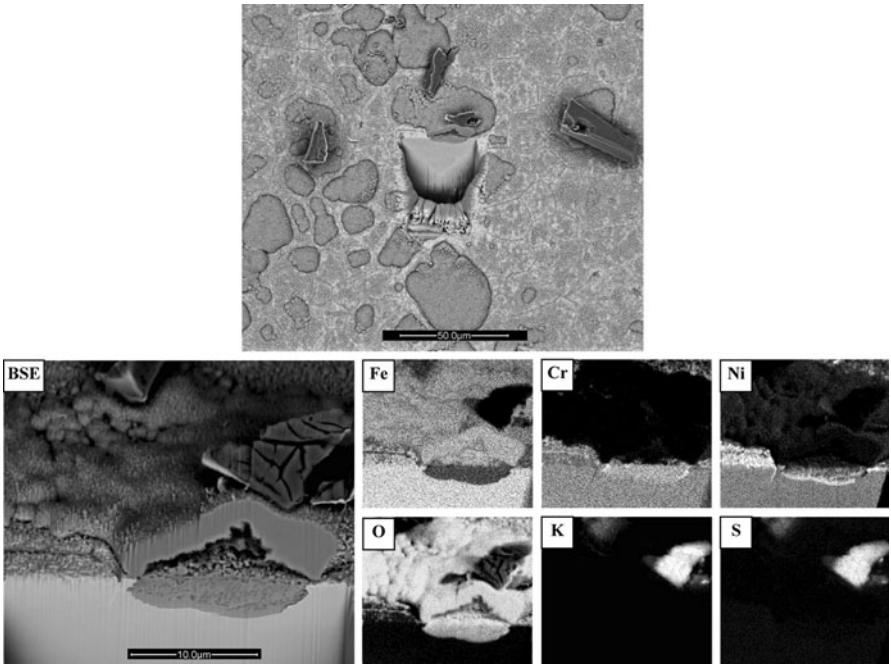

Fig. 7 52° Tilted FIB cross section of a sample exposed at 600 °C in $O_2 + H_2O + K_2SO_4$ for 24 h. *Top*: Overview BSE image. Micron bar corresponds to 50 µm. *Bottom*: SEM/EDX maps of the cross section. Micron bar corresponds to 10 µm

corrosion of stainless steels is played by the cation and not by the anion, as is often surmised. Hence, in both cases a thick duplex scale forms, featuring an outer layer consisting of hematite with scattered potassium chromate particles on top and an inner layer consisting of (Fe, Cr, Ni) spinel type oxide. The two oxide layers are separated by a straight interface corresponding to the original metal surface. It can be concluded that the outer layer has grown outward by cation diffusion while the inner layer has grown inward by oxygen ion diffusion. This corrosion morphology is referred to as "Type A". The "Type B" corrosion morphology is only observed with KCl. It designates the accumulation of corrosion products (mainly iron oxide) around the KCl crystallites. Thus, the samples exposed to K_2CO_3 only exhibit "Type A" morphology. The results show the formation of an oxide shell or rim of approximately the same size as the original KCl crystallites, see Fig. 4. The Type B morphology has been described by Jonsson et al. [24] and Pettersson [25] in the case of 304L and by Proff et al. [26] in the case of Sanicro 28 (a highly alloyed austenitic stainless steel, 35% Fe, 27% Cr, 31% Ni, 4% Mo and 2% Mn). According to [24, 25] the agglomerates form quite rapidly, 10 µm thick accumulations of oxide appearing already after 1 h at 600 °C. While the morphology of these formations is variable there is usually a shell-like structure, approximating the shape of the original salt particle with additional large funnel-shaped features often being present. FIB cross sectioning showed that the iron oxide aggregates are not

associated with a preferential (localized) corrosion attack of the steel. This means that the metal ions (mainly Fe) forming the oxide rim have originated far away from the KCl crystallite, implying fast lateral transport of ions on the sample surface. Because of the absence of localized attack in connection to the "Type B" morphology it is considered to be of secondary importance from the corrosion point of view. In the following, the "Type A" corrosion will be given most attention.

The available evidence shows that in "Type A" corrosion, breakdown of the protective oxide is triggered by the formation of potassium chromate(VI) [27]:

$$\tfrac{1}{2}Cr_2O_3(s) + 2KCl(s) + H_2O(g) + \tfrac{3}{4}O_2(g) \leftrightarrow K_2CrO_4(s) + 2HCl(g)$$
$$\Delta G_f^\circ = 74\,\text{kJ/mol}, p_{eq}(HCl) = 1.3 \times 10^{-3}\,\text{bar}\ (600\,^\circ\text{C}, pO_2 : 0.05\,\text{bar}, pH_2O{:}0.4\,\text{bar}) \quad (1)$$

$$\tfrac{1}{2}Cr_2O_3(s) + K_2CO_3(s) + \tfrac{3}{4}O_2(g) \leftrightarrow K_2CrO_4(s) + CO_2(g)$$
$$\Delta G_f^\circ = -129\,\text{kJ/mol}, p_{eq}(CO_2) = 5.2 \times 10^6\,\text{bar}\ (600\,^\circ\text{C}, pO_2 : 0.05\,\text{bar}) \quad (2)$$

In contrast to KCl and K_2CO_3, K_2SO_4 does not accelerate the corrosion of 304L, the same type of attack being observed as in the absence of salt, see Fig. 4. The non-corrosive nature of K_2SO_4 is explained by its relative thermodynamic stability. Hence, in contrast to KCl and K_2CO_3, the reaction of K_2SO_4 with the protective oxide to form K_2CrO_4 is not thermodynamically favoured in the present experimental conditions [27]:

$$\tfrac{1}{2}Cr_2O_3(s) + K_2SO_4(s) + \tfrac{3}{4}O_2(g) \rightarrow K_2CrO_4(s) + SO_3(g)$$
$$\Delta G_f^\circ = 135\,\text{kJ/mol}, p_{eq}(SO_3) = 8.9 \times 10^{-10}\,\text{bar}\ (600\,^\circ\text{C}, pO_2 : 0.05\,\text{bar}) \quad (3)$$

Hence, the observation that KCl and K_2CO_3 form chromate on the stainless steel surface while K_2SO_4 does not, is in accordance with the thermodynamics of the reactions, showing that the corrosivity of the three salts is directly coupled to the tendency for the salt to form chromate and deplete the protective oxide in chromia. The very low equilibrium pressure of $SO_3(g)$ means that the rate of reaction (3) has to be very low, reaction rate being limited by the rate of transport of $SO_3(g)$ in the gas phase.

The increased corrosion at 600 °C, in comparison to dry oxygen, observed in the $O_2 + H_2O$ and $O_2 + H_2O + K_2SO_4$ exposures can be attributed to the presence of water vapour. It is well-known that gas mixtures containing water vapour and oxygen react with chromia at high temperature forming chromic acid, $CrO_2(OH)_2(g)$ [27]:

$$\tfrac{1}{2}Cr_2O_3(s) + H_2O(g) + \tfrac{3}{4}O_2(g) \leftrightarrow CrO_2(OH)_2(g)$$
$$\Delta G_f^\circ = 105\,\text{kJ/mol}, p_{eq}\left(CrO_2(OH)_2\right) = 0.02 \times 10^{-6}\,\text{bar}$$
$$(600\,^\circ\text{C}, pO_2 : 0.05\,\text{bar}, pH_2O : 0.4\,\text{bar}) \quad (4)$$

As stated in the introduction, any process that depletes the protective oxide in chromium tends to makes it less protective and can trigger greatly accelerated corrosion. The corrosion accelerating effect of (4) on the high temperature corrosion of stainless steel has been demonstrated in several papers [1–4, 28–30]. To illustrate the significance of this mechanism, it may be noted that the oxidation behaviour of

304L stainless steel in a pure $O_2 + H_2O$ environment at 600 °C depends on flow rate. Thus, it has been reported that a steel that remained in the protective state at low gas flow rate could be forced into breakaway oxidation by simply increasing the flow rate. This is explained by the flow rate dependence of the evaporation of chromic acid from the protective oxide (reaction (4)) [30]. In the case of austenitic stainless steels such as 304L, chromium loss, by reaction (4), tends to trigger a local breakdown of the protective oxide. Hence, only the central parts of the steel grains are affected, the area in the vicinity of the grain boundaries remaining protective. As a result, oxide nodules form consisting of an outer hematite part and an inner part consisting of FeCrNi spinel oxide [4]. The present results regarding 304L exposed to $O_2 + H_2O$ at 600 °C in the absence of salt are in excellent agreement with the previously reported results, showing breakdown of the protective oxide on the middle of the steel grains, the resulting oxide nodules exhibiting the characteristic duplex island/crater morphology.

Considering the similarities between alkali chromate formation (1, 2) and chromic acid vaporization (4) one may expect the corrosion effects of the reactions to be analogous. Indeed, this expectation is corroborated by the present results, showing striking similarities between the duplex scale structures developed in $O_2 + H_2O$ in the absence of salt and in the presence of KCl and K_2CO_3. The main difference is that while the presence of KCl and K_2CO_3 resulted in general corrosion, exposure to $O_2 + H_2O$ in the absence of salt only resulted in a local breakdown of the protective oxide. Also, in the absence of KCl and K_2CO_3 corrosion only occurred at 600 °C and not at 500 °C.

The results show that, in contrast to $O_2 + H_2O$ in the absence of salts, KCl and K_2CO_3 are also efficient corrosion agents at 500 °C. Although the reaction is considerably slower compared to 600 °C, the composition of the corrosion products and the morphology of the corroded surface are essentially the same. Hence, we may conclude that the same corrosion mechanisms are active at 500 and 600 °C, involving chromium depletion of the protective oxide by potassium chromate formation and the subsequent breakaway oxidation of the steel. As noted above, exposure to $O_2 + H_2O$ at 500 °C in the absence of KCl and K_2CO_3 did not cause an enhanced corrosion rate. This is in accordance with earlier investigations on FeCr alloys [3, 29]. The slight effect of water vapour in this case is attributed to insignificant rate of vaporization of chromic acid. For the same reason, the $O_2 + H_2O + K_2SO_4$ exposure at 500 °C also did not give rise to an increased corrosion rate.

Conclusions

The present study shows that K_2CO_3 is equally corrosive as KCl towards 304L stainless steel at 500 and 600 °C. This proves that the crucial role in accelerating corrosion is played by the cation and not by the anion, as is often surmised. KCl and K_2CO_3 both react with the chromium-rich oxide on the steel surface, forming K_2CrO_4. The resulting chromium depletion of the protective oxide causes rapid oxidation and the formation of a thick duplex scale consisting of an upper hematite

layer and a lower layer made up of FeCrNi spinel-type oxide. The corrosion attack induced by the two potassium salts is analogous to that observed in $O_2 + H_2O$ environment in the absence of salt. In the latter case the accelerated corrosion attack is triggered by chromium depletion caused by the vaporization of chromic acid. However, while the latter environment causes local failure of the protective oxide, exposure to the two salts results in general corrosion. Also, corrosion only occurred at 600 °C and not at 500 °C in the absence of KCl and K_2CO_3. In contrast, K_2SO_4 has little influence on the corrosion rate and on the morphology of the corroded surface. The differences in the corrosivity of the three salts are directly connected to their ability to form chromate on the surface and, hence, to the relative stability of the corresponding leaving groups (HCl, CO_2 and SO_3).

Acknowledgment This work was carried out within the High Temperature Center (HTC) at Chalmers University of Technology.

References

1. H. Asteman, J. E. Svensson, L. G. Johansson and M. Norell, *Oxidation of Metals* **52**, 95 (1999).
2. H. Asteman, J. E. Svensson, M. Norell and L. G. Johansson, *Oxidation of Metals* **54**, 11 (2000).
3. K. Segerdahl, J.-E. Svensson and L.-G. Johansson, *Materials and Corrosion* **53**, 479 (2002).
4. M. Halvarsson, J. E. Tang, H. Asteman, J.-E. Svensson and L.-G. Johansson, *Corrosion Science* **48**, 2014 (2006).
5. N. Folkeson, J. Pettersson, C. Pettersson, L.-G. Johansson, E. Skog and J.-E. Svensson, *Materials Science Forum* **595–598**, 289 (2008).
6. J. Pettersson, C. Pettersson, N. Folkeson, L.-G. Johansson, E. Skog and J.-E. Svensson, *Materials Science Forum* **522–523**, 563 (2006).
7. B. M. Jenkins, L. L. Baxter and T. R. Miles, *Fuel Processing Technology* **54**, 1998 (17).
8. T. R. Miles, L. L. Baxter, R. W. Bryers, B. M. Jenkins and L. L. Oden, *Biomass & Bioenergy* **10**, 125 (1996).
9. H. J. Grabke, E. Reese and M. Spiegel, *Corrosion Science* **37**, 1023 (1995).
10. H. P. Nielsen, F. J. Frandsen, K. Dam-Johansen and L. L. Baxter, *Progress in Energy and Combustion Science* **26**, 283 (2000).
11. Y. Shu, F. Wang and W. Wu, *Oxidation of Metals* **51**, 97 (1999).
12. M. Spiegel, C. Schroer and H. J. Grabke, *Materials Science Forum* **251–254**, 527 (1997).
13. C. J. Wang and T. T. He, *Oxidation of Metals* **58**, 415 (2002).
14. Y. Shinata, *Oxidation of Metals* **27**, 315 (1987).
15. B. J. Skrifvars, R. Backman, M. Hupa, K. Salmenoja and E. Vakkilainen, *Corrosion Science* **50**, 1274 (2008).
16. B. J. Skrifvars, M. Westen-Karlsson, M. Hupa and K. Salmenoja, *Corrosion Science* **52**, 1011 (2010).
17. M. Brostrom, H. Kassman, A. Helgesson, M. Berg, C. Andersson, R. Backman and A. Nordin, *Fuel Processing Technology* **88**, 1171 (2007).
18. P. Henderson, P. Szakalos, R. Pettersson, C. Andersson and J. Hogberg, *Materials and Corrosion* **57**, 128 (2006).
19. A. Pettersson, L. E. Amand and B. M. Steenari, *Fuel* **88**, 1758 (2009).
20. J. Pettersson, H. Asteman, J.-E. Svensson and L.-G. Johansson, *Oxidation of Metals* **64**, 23 (2005).
21. J. Pettersson, J. E. Svensson and L. G. Johansson, *Oxidation of Metals* **72**, 159 (2009).

22. C. Pettersson, J. Pettersson, H. Asteman, J. E. Svensson and L. G. Johansson, *Corrosion Science* **48**, 1368 (2006).
23. C. Pettersson, L. G. Johansson and J. E. Svensson, *Oxidation of Metals* **70**, 241 (2008).
24. T. Jonsson, J. Froitzheim, J. Pettersson, J.-E. Svensson, L.-G. Johansson and M. Halvarsson, *Oxidation of Metals* **72**, 213 (2009).
25. J. Pettersson, *Alkali Induced High Temperature Corrosion of Stainless Steel—Experiences from Laboratory and Field, in Department of Chemical and Biological Engineering*, (Chalmers University of Technology, Gothenburg, 2008), p. 84.
26. C. Proff, T. Jonsson, C. Pettersson, J. E. Svensson, L. G. Johansson and M. Halvarsson, *Materials at High Temperatures* **26**, 113 (2009).
27. I. Barin, *Thermodynamic Data of Pure Substances*, 3rd edn. (VCH, Weinheim, 1995).
28. T. Jonsson, S. Canovic, F. Liu, H. Asteman, J. E. Svensson, L. G. Johansson and M. Halvarsson, *Materials at High Temperatures* **22**, 231 (2005).
29. K. Segerdahl, J.-E. Svensson and L.-G. Johansson, *Materials and Corrosion* **53**, 247 (2002).
30. H. Asteman, J. E. Svensson and L. G. Johansson, *Oxidation of Metals* **57**, 193 (2002).